TECHNICAL RESEARCH REPORT

A Model of the Dynamics of a Lathe Toolpost that Incorporates Active Vibration Suppression

by B.A. Frankpitt

T.R. 95-84

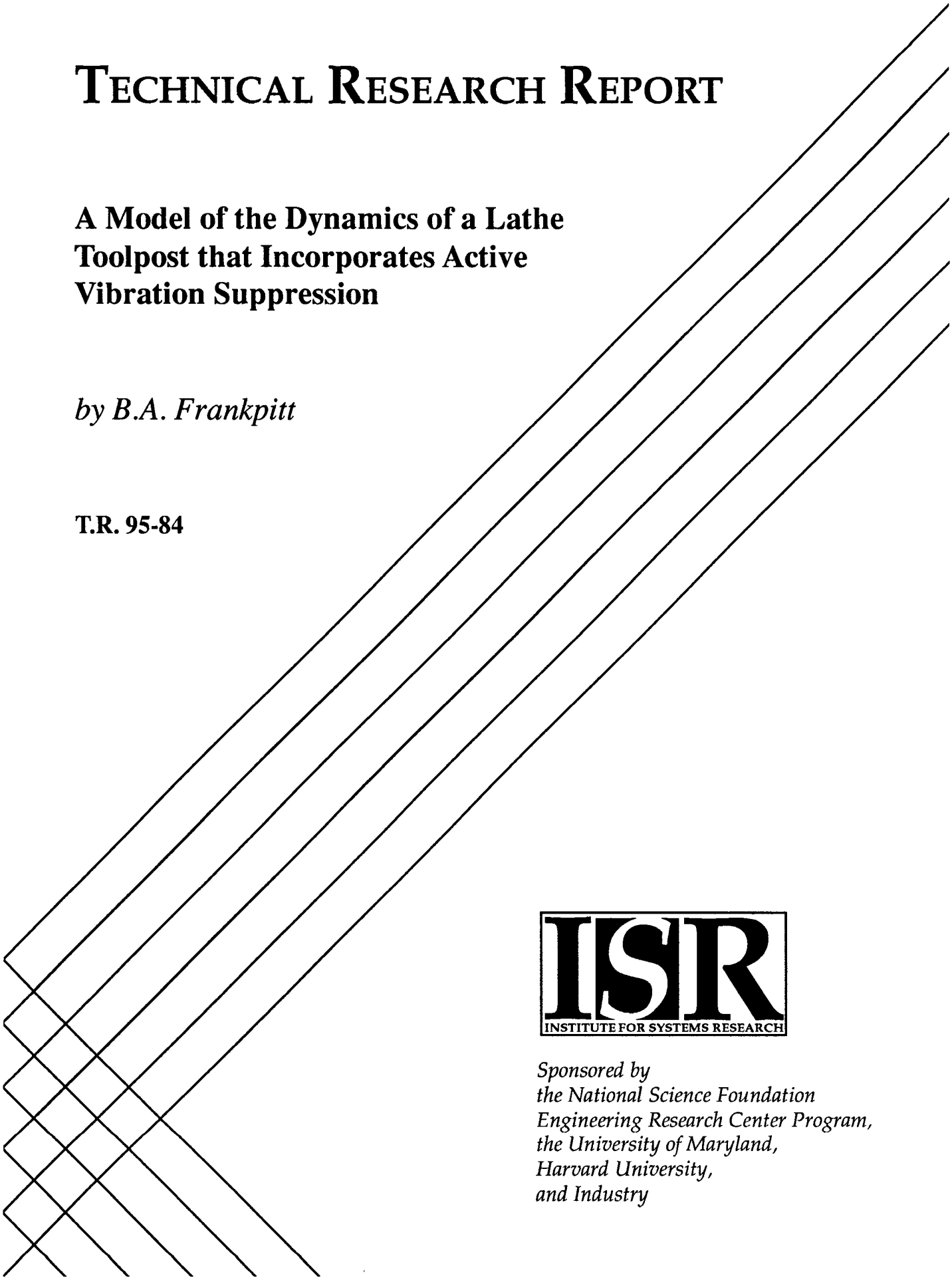

Sponsored by
the National Science Foundation
Engineering Research Center Program,
the University of Maryland,
Harvard University,
and Industry

A Model of the Dynamics of a Lathe Toolpost that Incorporates Active Vibration Suppression

B.A. Frankpitt

Institute for Systems Research
University of Maryland, College Park
Maryland, 20742 U.S.A.

ABSTRACT

A simple, linear, system model is presented for a lathe with a toolpost that incorporates active vibration suppression. The toolpost model is built from linear dynamic models of the component parts of the toolpost design: the actuator and drive circuitry, and the mechanical toolpost. The toolpost model is then combined with linear models for the lathe dynamics and cutting process to produce a model of the entire mechanical system. This model is used as the basis for a controller design that uses a measurement of the actuator current for a sensor signal, and the voltage applied to the actuator by the power amplifier as a control signal.

The controller design uses the H^{∞} design methodology. The performance criteria for the toolpost design are interpreted as measures on transfer functions associated with the system model, and predictions of the performance of the design are made on the basis of these measures. The conclusion drawn from this work is that with careful design, the active control of vibration in turning processes is a promising application for stack piezo-ceramic actuators.

1 INTRODUCTION

This report presents a simple, linear system model for the dynamics of a lathe toolpost that incorporates active vibration suppression. The toolpost described in the report was designed and built at the University of Maryland, College Park by Professor Guangming Zhang and his students during a project that was undertaken as a task under the ARPA SMS program[1]. This report presents the work that I have done on system modeling and controller design in conjunction with this project. The emphasis in the work is directed towards design issues rather than theoretical issues, and I have attempted to avoid theoretical technicality wherever possible. While much of the work is an application of well established design methodology, my approach to modeling the piezo-ceramic actuator as a linear two port system is not standard practice. This approach does offer the advantages that it potentially eliminates the need for an extra electro-mechanical motion sensor, and that it completely models the interactions between the mechanical and electrical components of the system within the framework of the linear assumptions.

The development of a system model is an important step in system design. A system model provides a means both to evaluate whether the proposed design is capable of meeting the design requirements and to determine which system components need precise characterization. A model can aid in understanding how decisions made in the design of system components affect the overall behavior of the entire system, as an illustration of this point, this report includes a controller design for the active toolpost that is based on the linear system model.

The starting point for establishing a system model has to be the objectives of the final design — the system model needs to be sufficiently powerful to determine whether the system design objectives are being met. In short the system design objective for the toolpost project is a demonstration that a machine fitted with an active toolpost produces a measurably better surface finish than a machine fitted with a conventional toolpost under identical machining conditions. The quality of a machined surface is related to the amplitude and direction of the vibrational motion of the tool tip relative to the workpiece. Motion of the tool tip in a direction normal to the workpiece surface produces variation in the depth of cut which appears in the final product as an irregularity in the surface finish. The goals of the system design are to minimize the component of the vibrational motion of the tool relative to the workpiece surface that lies in the direction that is normal to the workpiece surface, to maintain the tracking performance of the tool tip with respect to the low frequency signal that controls the depth of cut, and to maintain robust stability of the system about the equilibrium cut in the face of variations in the plant parameters.

Two explanations for the source of mechanical vibration seem pertinent to this problem. The first is that vibration is caused by exogenous disturbances such as prior surface roughness, inhomogeneities in the workpiece material, vibration transmitted through the lathe structure, or cutting force variations resulting from built up edge or other phenomena associated with the mechanics of the cutting process.

[1]ARPA Agreement No.: MDA972-93-H-0003

The second explanation is that the vibration is caused by non-linear system dynamics; that is to say that the system trajectory that corresponds to an equilibrium cut is unstable, and that the actual system trajectory is close to a stable limit cycle; a demonstration of a model exhibiting this type of behavior has been given in an earlier report. The two types of vibration generally exhibit quite different characteristics. A vibration that results from an exogenous disturbance will look like a filtered noise signal and typically will have broad spectral peaks and low phase coherence. A vibration that results from a system trajectory that follows a stable limit cycle will have a peaky spectrum with harmonics, and high phase coherence. (Exceptions to these tendencies include exogenous disturbances that are highly periodic, and nonlinear dynamics of systems with strange attractors.) Simultaneous control of both types of vibration leads to competing system design objectives. The effects of exogenous disturbances are diminished by increasing the open loop gain of the system, while the stability of equilibrium trajectories is generally maintained by keeping the open loop gain small.

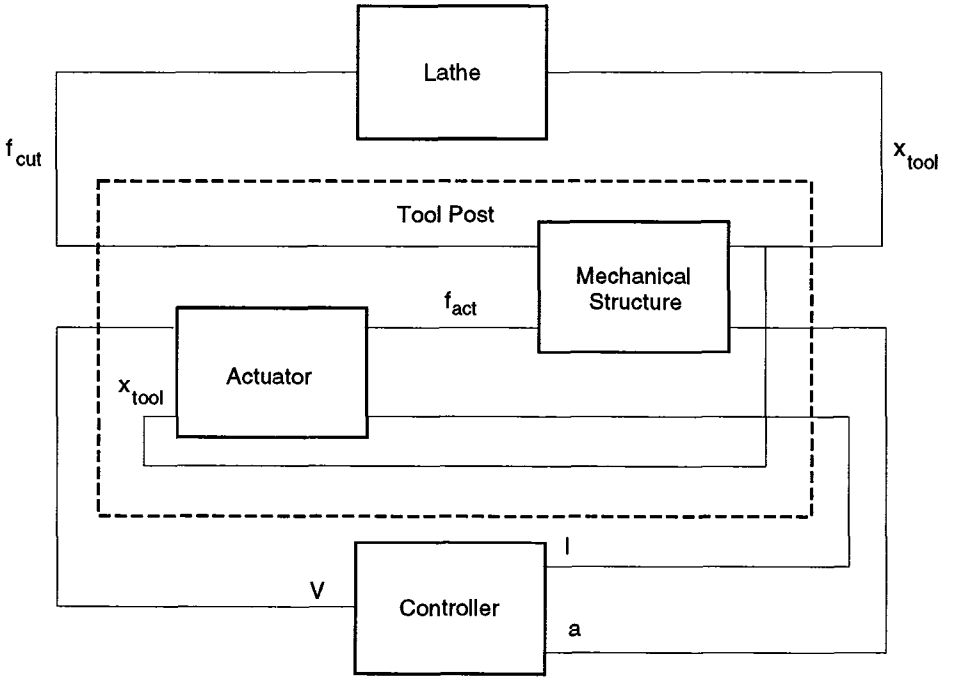

Figure 1. Schematic of System Dynamics.

An appropriate initial model for system design is a linear model with the structure illustrated in Fig 1. The linear model should be interpreted as representing the system dynamics linearized around a constant equilibrium trajectory representing a stable unperturbed cut. The reasons for the choice of this system structure

and the choices of the models for the system components are largely pragmatic — simple linear models are easy to work with and give good intuition as to where non-linearities in the system may be important. A second reason for choosing a simple model is that aspects of the system model such as the cutting process and the lathe dynamics are poorly defined or highly variable even within a single cutting task, consequently it does not make much sense to over-model the system and then tune the design for a particular system model when in fact the design should be robust to large variations in the system dynamics.

The remaining sections in the report describe the details of the models for the various system components, emphasis has been placed on providing both time domain and frequency domain descriptions of the linear sub-systems. While the time domain descriptions are important for simulation of the system, the transfer function matrices of the various components give a much better description of the system behavior. A controller design is computed, and an initial estimate of the expected system performance is made.

2 LINEAR MODEL FOR ACTUATOR AND DRIVE CIRCUIT

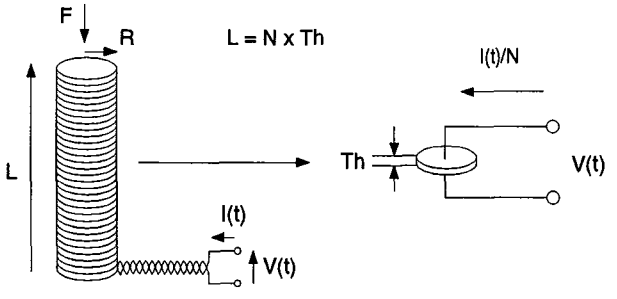

Figure 2. Detail of Actuator Geometry.

This section presents a simple linear model for the actuator based on linear constitutive equations for a piezo-electric material. It is assumed that the actuator is lossless. The geometry of the actuator is defined in Figure 2, and in addition the cross-sectional area is denoted by $\mathcal{A} = \pi R^2$. The constitutive parameters are the relative permitivity K, the Young's modulus Y, and the parameter g which is defined by the expression

$$\begin{aligned} g &= \left.\frac{\text{strain developed}}{\text{applied charge density}}\right|_{\text{free mechanical boundary}} \\ &= \left.\frac{\text{open circuit field}}{\text{applied stress}}\right|_{\text{open circuit electrical boundary}}. \end{aligned}$$

The parameter g is related to the piezo-electric constant d by[2]

$$g = \frac{d}{K\epsilon_0}.$$

A model for the actuator that expresses the extension of the actuator and the voltage across the actuator in terms of the force applied to the actuator and the total charge produced on the positive electrodes is given by

$$\begin{bmatrix} x \\ V \end{bmatrix} = \begin{bmatrix} P_{11} & P_{12} \\ P_{21} & P_{22} \end{bmatrix} \begin{bmatrix} f \\ Q \end{bmatrix} \tag{1}$$

in which

$$P_{11} = -\frac{L}{\mathcal{A}Y} \qquad P_{12} = \frac{L}{N\mathcal{A}}\frac{d}{K\epsilon_0}$$
$$P_{21} = \frac{L}{N\mathcal{A}}\frac{d}{K\epsilon_0} \qquad P_{22} = \frac{L}{N^2\mathcal{A}}\frac{1}{K\epsilon_0}.$$

Note that

$$P_{22} = \left.\frac{1}{\text{capacitance}}\right|_{\text{free mechanical boundary}}$$
$$P_{11} = -\left.\frac{1}{\text{stiffness}}\right|_{\text{open circuit electrical boundary}}$$

From the point of view of control system design it is more convenient to consider the extension of the actuator x and the voltage across the actuator V_{act} as the inputs to the actuator, and force produced by the actuator f_{act} and the current entering the actuator I_{act} as the outputs. However, considering the current as an output results in an improper transfer-function matrix, a difficulty that is resolved with the realization that that the voltage and current on the electrical side of the actuator can not be determined independently, but are constrained by the characteristics of the drive circuitry. In particular, the output impedance of the amplifier which is connected in parallel with the electrical impedance of the actuator greatly influences the transfer function of the combined actuator-drive circuitry. Consequently a simple model of the drive amplifier needs to be included in the system model; Figure 3 contains an appropriate circuit.

In addition to the piezo-electric equation (1), the equations for the model are

$$V_s = A_{\text{ol}}\left(\frac{R_2 V_{\text{in}} - R_1 V_{\text{act}}}{R_1 + R_2}\right)$$
$$V_{\text{act}} = V_s - I_{\text{act}} R_s$$
$$I_{\text{act}} = \frac{d}{dt} Q_{\text{act}}.$$

[2] $\epsilon_0 = 8.85 \times 10^{-12} Fm^{-1}$

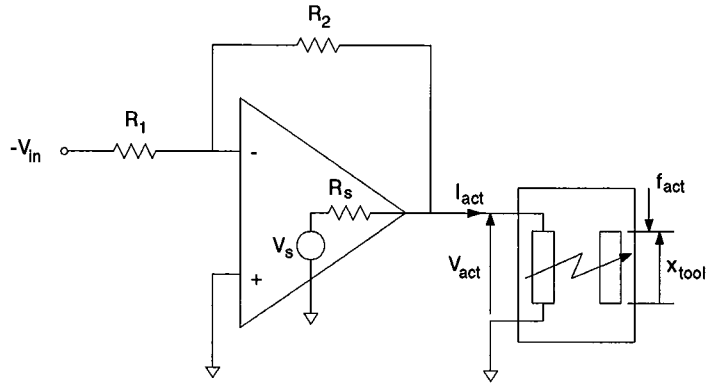

Figure 3. Electrical schematic of actuator and drive circuitry

These reduce to two equations

$$\begin{aligned} R_s\dot{Q}_{\rm act} + \left(1 + A_{\rm ol}\frac{R_1}{R_1+R_2}\right)\left(P_{22} - \frac{P_{12}P_{21}}{P_{11}}\right)Q_{\rm act} \\ = A_{\rm ol}\frac{R_2}{R_1+R_2}V_{\rm in} - \left(1 + A_{\rm ol}\frac{R_1}{R_1+R_2}\right)\frac{P_{21}}{P_{11}}x_{\rm act} \\ f_{\rm act} = \frac{x_{\rm act}}{P_{11}} - \frac{P_{12}}{P_{11}}Q_{\rm act}, \end{aligned}$$

which yield a state-space model for the actuator of the form

$$\begin{aligned} \dot{\zeta}_{\rm act} &= A_{\rm act}\zeta_{\rm act} + B_{\rm act}u_{\rm act} \\ y_{\rm act} &= C_{\rm act}\zeta_{\rm act} + D_{\rm act}u_{\rm act} \end{aligned}$$

with

$$\zeta_{\rm act} = [Q_{\rm act}], \quad u_{\rm act} = \begin{bmatrix} x \\ V_{\rm in} \end{bmatrix}, \quad y_{\rm act} = \begin{bmatrix} f_{\rm act} \\ I_{\rm act} \end{bmatrix}$$

and

$$\begin{aligned} A_{\rm act} &= \left[\frac{-L}{R_sN^2\mathcal{A}K^2\epsilon_0^2}(K\epsilon_0 + d^2Y)\left(1 + A_{\rm ol}\frac{R_1}{R_1+R_2}\right)\right] \\ B_{\rm act} &= \left[\frac{dY}{R_sNK\epsilon_0}\left(1 + A_{\rm ol}\frac{R_1}{R_1+R_2}\right) \quad \frac{A_{\rm ol}}{R_s}\frac{R_2}{R_1+R_2}\right] \\ C_{\rm act} &= \begin{bmatrix} \dfrac{dY}{NK\epsilon_0} \\ \dfrac{-L}{R_sN^2\mathcal{A}K^2\epsilon_0^2}(K\epsilon_0 + d^2Y)\left(1 + A_{\rm ol}\dfrac{R_1}{R_1+R_2}\right) \end{bmatrix} \end{aligned}$$

$$D_{\text{act}} = \begin{bmatrix} \dfrac{\mathcal{A}Y}{L} & 0 \\ \dfrac{dY}{R_s N K \epsilon_0}\left(1 + A_{\text{ol}}\dfrac{R_1}{R_1+R_2}\right) & \dfrac{A_{\text{ol}}}{R_s}\dfrac{R_2}{R_1+R_2} \end{bmatrix}.$$

3 MODELLING THE TOOLPOST

The dynamics of the mechanical toolpost structure are modeled by the simple mass-spring system illustrated in Figure 4. The force from the ceramic actuator acts in parallel with the cutting force on the rigid body, mass M_1, to which the cutting tool is attached. The spring K_1 and the damping C_1 model the membrane spring that supports the mass M_1.

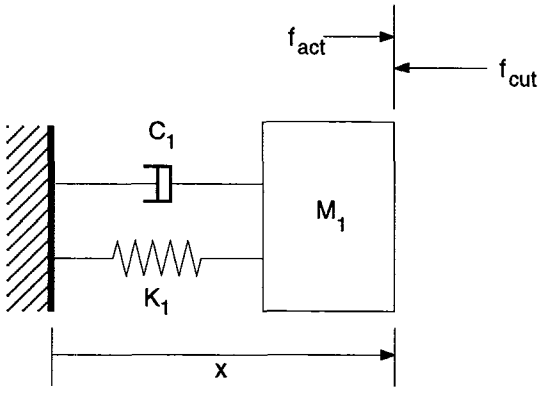

Figure 4. Mechanical Schematic for a Linear Model of the Tool-Post

The equation of motion for the dynamics of the linear tool-post model is

$$0 = f_{\text{cut}} - f_{\text{act}} + K_1 x_1 + C_1 \dot{x} + M_1 \ddot{x}, \tag{2}$$

which yields a system of state equations

$$\dot{x}_{\text{tool}} = A_{\text{tool}} x_{\text{tool}} + B_{\text{tool}} u_{\text{tool}}$$

in which the state vector and input vector are given by

$$x_{\text{tool}} = \begin{pmatrix} \dot{x} \\ x \end{pmatrix} \qquad u_{\text{tool}} = \begin{pmatrix} f_{\text{cut}} \\ f_{\text{act}} \end{pmatrix},$$

and the matrices A_{tool} and B_{tool} are given by

$$A_{\text{tool}} = \begin{pmatrix} -\frac{C_1}{M_1} & -\frac{K_1}{M_1} \\ 1 & 0 \end{pmatrix}$$

$$B_{\text{tool}} = \begin{pmatrix} \frac{-1}{M_1} & \frac{1}{M_1} \\ 0 & 0 \end{pmatrix}.$$

The output vector from the model is

$$y_{\text{tool}} = \begin{pmatrix} x_{\text{tool}} \\ a \end{pmatrix}$$

which has components a, the signal from an accelerometer attached to the mass M_1, and x_{tool}, the position of M_1. The output equation is

$$y_{\text{tool}} = C_{\text{tool}} x_{\text{tool}} + D_{\text{tool}} u_{\text{tool}}$$

in which the matrices C_{tool} and D_{tool} are given by

$$C_{\text{tool}} = \begin{pmatrix} 0 & 1 \\ -\frac{C_1}{M_1} & -\frac{K_1}{M_1} \end{pmatrix}$$

$$D_{\text{tool}} = \begin{pmatrix} 0 & 0 \\ \frac{-1}{M_1} & \frac{1}{M_1} \end{pmatrix}.$$

The transfer function for the system is found by taking the Laplace transform of equation (2) and ignoring the initial conditions, this gives:[3]

$$0 = \hat{f}_{\text{cut}} - \hat{f}_{\text{act}} + sC_1\hat{x} + K_1\hat{x} + s^2 M_1 \hat{x}. \tag{3}$$

Solving for $\hat{x}_1$ in terms of the input signals $\hat{f}_{\text{cut}}$ and $\hat{f}_{\text{act}}$ gives

$$\hat{x} = \frac{\hat{f}_{\text{act}} - \hat{f}_{\text{cut}}}{Ms^2 + Cs + K}.$$

The transfer functions with respect to the two input forces differ only in sign; each has a pair of poles at

$$s = \frac{-C_1 \pm \sqrt{C_1^2 - 4K_1M_1}}{2M_1}.$$

The model for the mechanical part of the toolpost may be combined with the model for the actuator to give a transfer function matrix that relates the tool displacement $\hat{x}_{\text{tool}}$, the acceleration measurement $\hat{a}$ and the actuator current measurement $\hat{I}$ to the cutting force $\hat{f}_{\text{cut}}$ and the voltage signal applied to the actuator drive amplifier $\hat{V}_{\text{in}}$.

$$\begin{bmatrix} \hat{x}_{\text{tool}}(s) \\ \hat{a}(s) \\ \hat{I}(s) \end{bmatrix} = \begin{bmatrix} t_{11}(s) & t_{12}(s) \\ t_{21}(s) & t_{22}(s) \\ t_{31}(s) & t_{32}(s) \end{bmatrix} \begin{bmatrix} \hat{f}_{\text{cut}}(s) \\ \hat{V}_{\text{in}} \end{bmatrix}. \tag{4}$$

Appendix A contains a MATLAB[4] script for the Toolpost model, and Bode plots of the elements of the transfer function matrix $t_{11}(s) \ldots t_{32}(s)$ are presented in Figure

[3] A hat over a signal indicates the Laplace transform of the signal, so $\hat{f}$ is the the Laplace transform of the force signal f.

[4] MATLAB is a trademark of The MathWorks Inc.

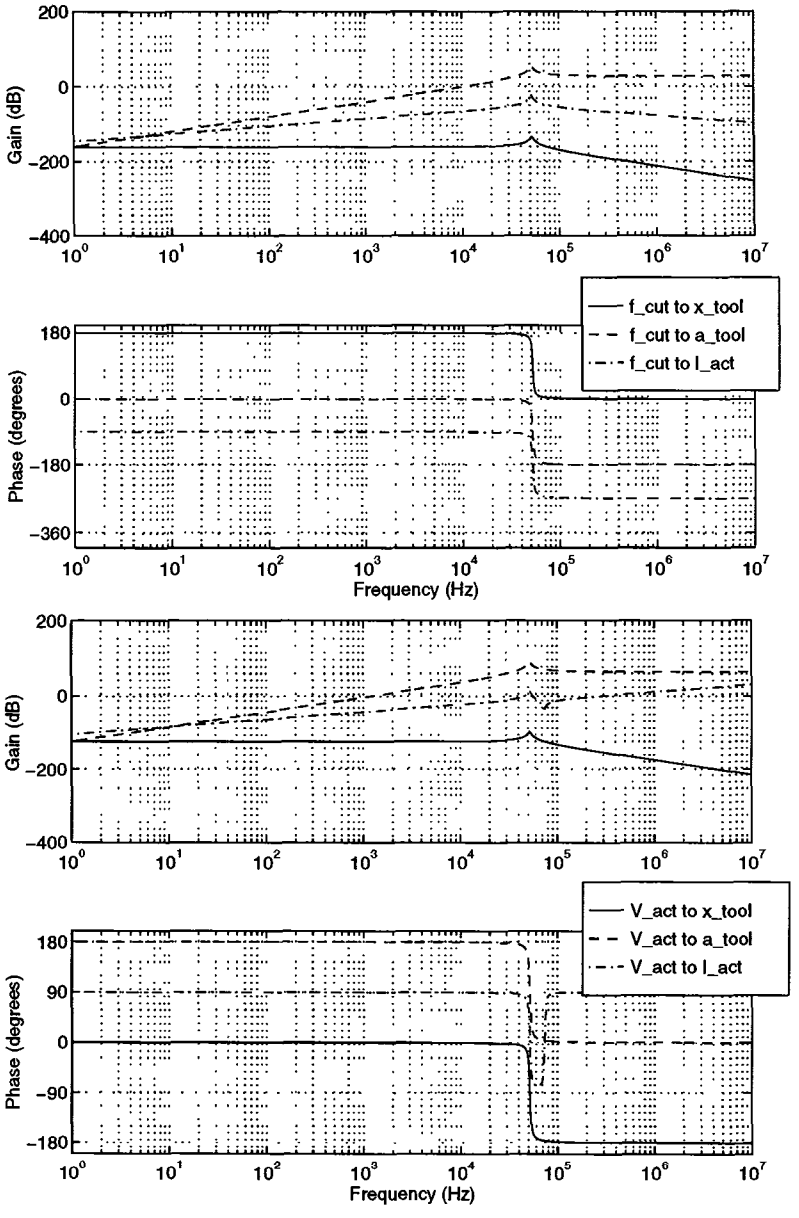

Figure 5. Bode plots of transfer functions for toolpost structure

5. The model parameters that were used for these plots are given in Table 1. The model parameters that quantify constitutive properties of the piezo-ceramic material are taken from Vernitron data sheets for PZT ceramics. The geometric parameters were measured or guessed from sample actuators produced by AVX. The stiffness K_{act} that appears in Table 1 is the open circuit stiffness of the actuator and is given by the formula

$$K_{\text{act}} = \frac{\pi R^2 K \epsilon_0 Y}{LK\epsilon_0 + d^2 Y}.$$

Parameter	Value
Actuator Parameters	
L	1.8×10^{-2}
R	3.5×10^{-3}
N	150
K	1300
d	350×10^{-12}
Y	9.9×10^{10}
Drive Circuitry Parameters	
A_{ol}	10^5
R_1	$2 \times 10^3 \Omega$
R_2	$28 \times 10^3 \Omega$
R_s	10Ω
Toolpost Structure Parameters	
M_1	$0.2\ Kg$
M_2	$0.04\ Kg$
K_1	$K_{\text{act}}/10\ N/m$
K_2	$K_{\text{act}}/100\ N/m$
ξ_1	0.03
ξ_2	0.03

Table 1. Parameters for model of toolpost and actuator dynamics

If the controller is assumed to take the form

$$\hat{V}_{\text{in}}(s) = Q_1(s)\hat{a}(s) + Q_2(s)\hat{I}(s)$$

then the transfer function of the combined toolpost with controller may be written as $\hat{x}_{\text{cut}}(s) = T_{\text{tool}}(s)\hat{f}_{\text{cut}}(s)$ with

$$T_{\text{tool}}(s) = t_{11}(s) + t_{12}(s)\frac{t_{21}(s)Q_1(s) + t_{31}(s)Q_2(s)}{1 - t_{22}(s)Q_1(s) - t_{32}(s)Q_2(s)}. \tag{5}$$

4 MODEL OF LATHE

The model for the lathe presented in this section is a simple model based on the ideas of Merritt [4] who models the turning process with a dynamic system that is

composed of three parts. The first part is a kinematic equation that expresses the chip load $u(t)$ as a function of $y(t)$ and $y(t-\tau)$, the distances between the tool tip and the center of the workpiece at successive revolutions of the workpiece.[5]

$$u(t) = y(t) - \mu y(t-\tau) \tag{6}$$

In this equation τ denotes the transport delay associated with one revolution of the workpiece, and μ is the overlap factor which is a function of the feed-rate and the period of a revolution T.

The second part of the model is the relationship between the cutting force f_{cut} and the chip load $u(t)$. It is to be expected that an accurate characterization of this relationship would involve a complicated non-linear model of the cutting process, but as a first approximation the variation in cutting force is assumed to be proportional to the variation in the depth of cut and is given by the linear equation

$$f_{\text{cut}}(t) = -k_c u(t). \tag{7}$$

The value for k_c depends on a variety of factors including tool geometry, the material composition of the workpiece and the equilibrium value of the depth of cut. In any specific instance k_c is calculated from an empirical model; this report uses a model from The PhD dissertation of Zhang [5]. Zhang gives the relationship

$$k_c = \frac{7500 \times d}{f^{0.15} \times N^{0.05}}$$

for the cutting stiffness of a standard diameter aluminum test piece as a function of cutting speed N (in rpm), depth of cut d (in mm), and feedrate f (in mm/revolution). The values used for N, f, and d in the model are

$$N = 2400 \qquad f = 1.5 \qquad d = 5.$$

The third part of the model is a description of the dynamics of the mechanical systems that comprise the lathe and the workpiece. Merritt assumes that the tool-post is infinitely rigid, and describes the lathe dynamics with a linear n-degree of freedom model. Here, a linear model that combines the dynamics of the mechanical toolpost design with the dynamics of the controller is used to describe the behavior of the toolpost, and a single degree of freedom model is used to describe the behavior of the lathe and workpiece. The lathe model may be interpreted as a model of the first resonant mode of the combined lathe workpiece structure; with this interpretation the lathe model is expressed by the equation

$$f_{\text{cut}}(t) = M\ddot{x}_{\text{lathe}}(t) + C\dot{x}_{\text{lathe}}(t) + Kx_{\text{lathe}}(t), \tag{8}$$

where M, C, and K denote the effective mass, stiffness and damping coefficients of the dominant mode.

[5] All variables should be interpreted as variations around an equilibrium value that corresponds to a (possibly unstable) equilibrium cut.

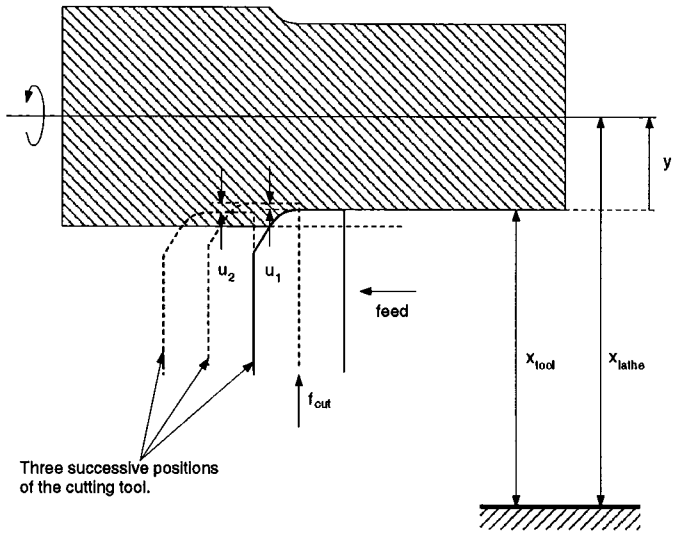

Figure 6. Detail of Cutting Process.

Figure 6 illustrates the the relationship between the mechanical signals that describe the cutting process. In the figure the position of the workpiece, x_{lathe} is kept constant in successive rotations in order to keep the illustration simple. The variable y is the difference in the positions of the tool tip and the workpiece.

$$y = x_{\text{lathe}} - x_{\text{tool}}. \tag{9}$$

The signal associated with this variable represents the variation in surface height of the machined workpiece along a curve that traces the path of the tool tip on the workpiece, and which is parameterized by the cutting speed. This signal is important in the evaluation of the design because variations in $y(t)$ represents variations in the surface height, and therefore quality, of the machined surface.

Figure 7 is a schematic of the dynamics of the combined system of lathe and toolpost. A disturbance f_{dist} is introduced as a pair of forces of equal magnitude acting in opposite directions on the workpiece surface and the tool tip. A low frequency control signal x_{cont} is introduced as an offset on the position of the tool tip. Varying x_{cont} varies the depth of cut. The toolpost, which includes the controller, is modeled by a linear system with transfer function T_{tool} that relates the signals f_{cut}, x_{cont} and x_{tool} by the equation

$$\hat{x}_{\text{tool}} = \hat{x}_{\text{cont}} + T_{\text{tool}}\hat{f}_{\text{cut}}.$$

Equations for the lathe model are derived from Figure 7 as follows. Balancing

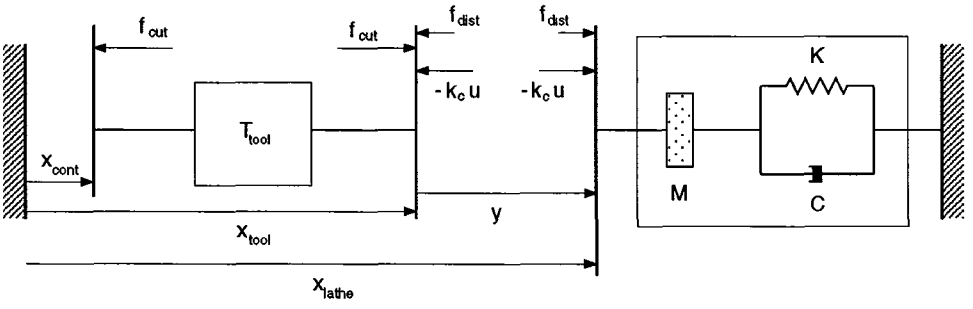

Figure 7. Mechanical schematic of lathe model with disturbances

forces on the mass M gives the equation

$$\hat{f}_{\text{dist}} - k_c\hat{u} = s^2M\hat{x}_{\text{lathe}} + sC\hat{x}_{\text{lathe}} + K\hat{x}_{\text{lathe}}, \tag{10}$$

And balancing forces at the tool tip gives

$$\hat{f}_{\text{dist}} - k_c\hat{u} = \hat{f}_{\text{cut}}. \tag{11}$$

Substituting (9) into (6) and taking Laplace transforms gives

$$\hat{u} = (1 - \mu e^{-s\tau})(\hat{x}_{\text{lathe}} - \hat{x}_{\text{tool}})$$

which, in turn may be substituted into (10) and (11) to give the pair of equations

$$\begin{aligned} \hat{f}_{\text{dist}} + k_c(1 - \mu e^{-s\tau})\hat{x}_{\text{tool}} &= (s^2M + sC + K + k_c(1 - \mu e^{-s\tau}))\hat{x}_{\text{lathe}} \\ \hat{f}_{\text{dist}} + k_c(1 - \mu e^{-s\tau})\hat{x}_{\text{tool}} &= \hat{f}_{\text{cut}} + k_c(1 - \mu e^{-s\tau}))\hat{x}_{\text{lathe}}. \end{aligned} \tag{12}$$

Eliminating $\hat{x}_{\text{lathe}}$ gives

$$\begin{aligned} \hat{f}_{\text{cut}} &= \frac{s^2M + sC + K}{s^2M + sC + K + k_c(1 - \mu e^{-s\tau})}\hat{f}_{\text{dist}} \\ &+ \frac{k_c(1 - \mu e^{-s\tau})(s^2M + sC + K)}{s^2M + sC + K + k_c(1 - \mu e^{-s\tau})}\hat{x}_{\text{tool}}. \end{aligned} \tag{13}$$

Recalling that $\hat{y} = \hat{x}_{\text{lathe}} - \hat{x}_{\text{tool}}$, a rearrangement of (12) gives

$$k_c(1 - \mu e^{-s\tau})\hat{y} = \hat{f}_{\text{dist}} - \hat{f}_{\text{cut}},$$

and substituting the equation for f_{cut} (13) gives

$$\hat{y} = \frac{1}{s^2M + sC + K + k_c(1 - \mu e^{-s\tau})}\hat{f}_{\text{dist}} - \frac{s^2M + sC + K}{s^2M + sC + K + k_c(1 - \mu e^{-s\tau})}\hat{x}_{\text{tool}}.$$

To summarize, the model for the Lathe may be written as

$$\begin{bmatrix} \hat{y} \\ \hat{f}_{\text{cut}} \end{bmatrix} = \begin{bmatrix} T_{11} & T_{12} \\ T_{21} & T_{22} \end{bmatrix} \begin{bmatrix} \hat{f}_{\text{dist}} \\ \hat{x}_{\text{tool}} \end{bmatrix}$$

with

$$T_{11}(s) = \frac{1}{s^2M + sC + K + k_c(1 - \mu e^{-s\tau})}$$

$$T_{12}(s) = \frac{-(s^2M + sC + K)}{s^2M + sC + K + k_c(1 - \mu e^{-s\tau})}$$

$$T_{21}(s) = \frac{s^2M + sC + K}{s^2M + sC + K + k_c(1 - \mu e^{-s\tau})}$$

$$T_{22}(s) = \frac{k_c(1 - \mu e^{-s\tau})(s^2M + sC + K)}{s^2M + sC + K + k_c(1 - \mu e^{-s\tau})}.$$

The delay in the lathe model prevents the model being written in terms of a differential equation on a finite dimensional state space. Rather than making a finite dimensional state-space approximation to the model, computations involving the lathe model are all performed in the frequency domain where the model is expressed by the transcendental transfer functions $T_{11} \ldots T_{22}$. The Matlab M-file that computes these transfer functions is given in Appendix B. The values of the model parameters that were used for the computations are given in Table 2, and the Bode plots for the lathe transfer functions are presented in Figure 8.

5 CONTROLLER DESIGN

The first problem that needs to be addressed in control system design is that of finding an appropriate way of representing the design objectives in terms of a computable measure on the system model. As mentioned in the introduction, the important criteria in the toolpost design are: performance of the system with respect to tracking the low bandwidth input that controls the depth of cut, rejection of the disturbances caused by perturbations in the cutting force, and robust stability of the closed loop system with respect to perturbations in the plant model. Following a traditional, frequency domain, H^∞ approach, these criteria are expressed

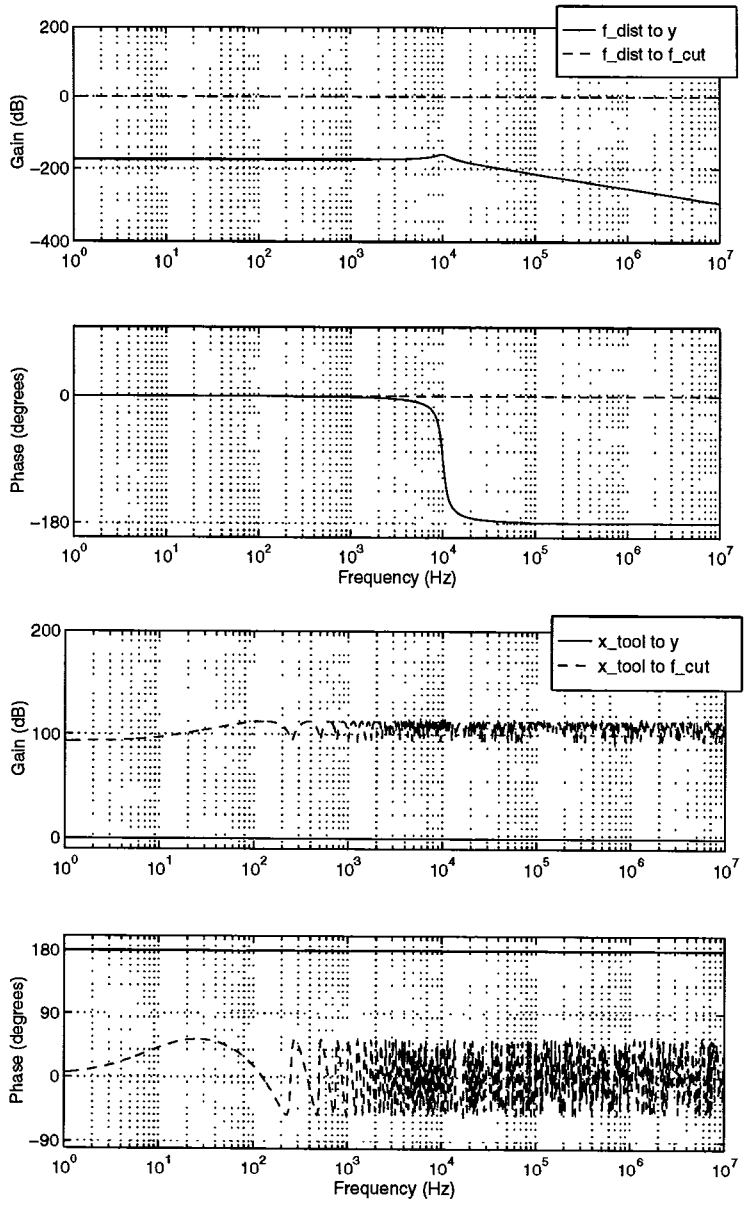

Figure 8. Transfer functions for model of Lathe

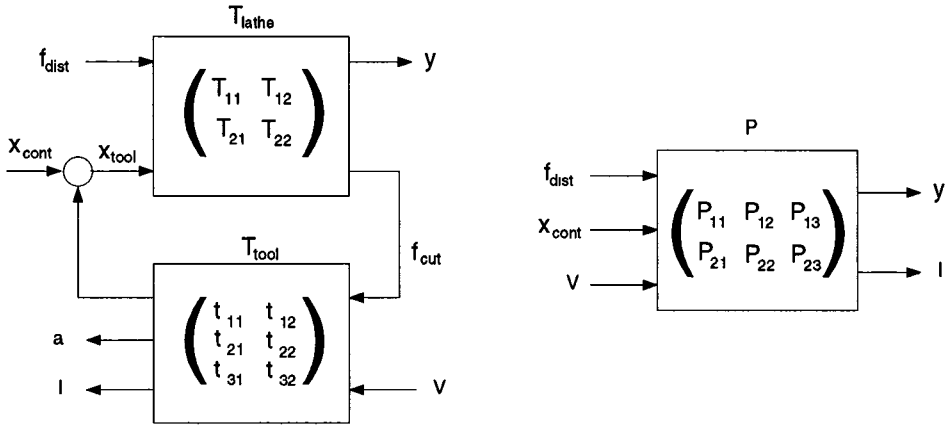

Figure 9. Signal Flow for Closed loop system with disturbances

Parameter	Value
k_c	$5.0 \times 10^8\ N/m$
τ	$0.02\ s$
μ	0.8
K	$5.0 \times 10^6\ N/m$
ω	$500\ rad/s$
ξ	0.03

Table 2. Parameters for Turning Process

within the linear theory that has been developed as measures on the magnitudes of appropriately selected closed loop transfer functions.

The linear system model for the toolpost and lathe is represented by the signal flow diagram on the left of Figure 9. The signals x_{cont} and f_{dist} are exogenous inputs to the system: the first models the low-bandwidth control signal, and the second models the higher frequency disturbances that perturb the cutting force. The signal y is the distance from the surface of the workpiece to the rotational axis. This signal determines system performance since variations in the radius of the workpiece appear as surface roughness in the finished workpiece. The signals a and I are the accelerometer and current sensor signals that are available to the controller, and the signal V is the actuator voltage signal that the controller regulates. From the toolpost model in Section 3, it is apparent that under the assumptions made when determining the linear model the acceleration signal a is proportional to the derivative of the current signal I. Consequently, observability of the plant is not lost by ignoring the signal a in a simplified initial design for the controller. In a final design, consideration of sensor noise, nonlinearity and dynamic range will determine what arrangement of the two sensors should be used. So, ignoring the acceleration signal, the dynamics of the toolpost without controller may be modeled by the three input, two output transfer function matrix on the right of Figure 9. The entries in the transfer function matrix, P_{11} to P_{23}, are given by the formulae

$$P_{11} = T_{11} + \frac{T_{12}t_{11}T_{21}}{(1 - t_{11}T_{22})} \qquad P_{12} = \frac{T_{12}t_{12}}{(1 - t_{11}T_{22})} \qquad P_{13} = \frac{T_{12}}{(1 - t_{11}T_{22})}$$
$$P_{21} = \frac{t_{31}T_{21}}{(1 - t_{11}T_{22})} \qquad P_{22} = t_{32} + \frac{t_{31}T_{22}t_{21}}{(1 - t_{11}T_{22})} \qquad P_{23} = \frac{t_{31}T_{22}}{(1 - t_{11}T_{22})}.$$

The performance of the controlled system is evaluated in terms of the closed loop transfer functions that relate the disturbance signal f_{dist} and the control signal x_{cont} to the measured output y. A design that performs well is one that achieves low gain between f_{dist} and y over the bandwidth where the spectral density of f_{dist} is large (frequencies between $100\,Hz$ and $5\,kHz$), yet maintains unity gain with π phase-shift between the signals x_{cont} and y over the bandwidth where the spectral density

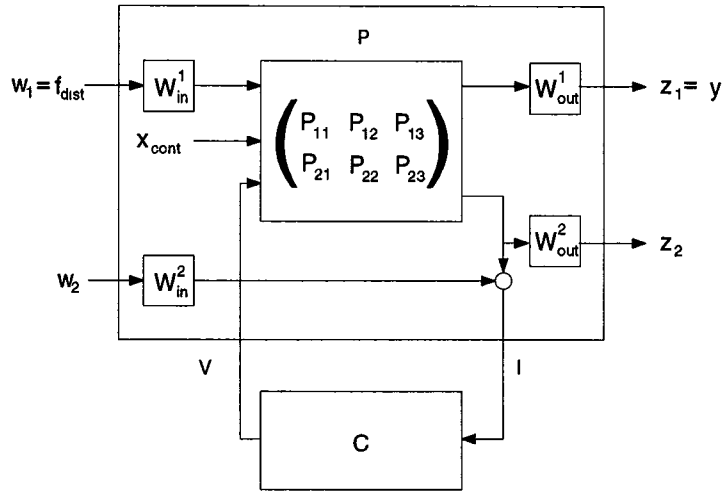

Figure 10. Configuration for Four Block H^∞ Problem

of the control signal x_{cont} is high (frequencies less than 3 Hz). In practice it is found that the second requirement, which is a tracking requirement, is easy to satisfy, and the effort in the controller design is directed towards meeting the first requirement which is a disturbance rejection requirement.

The H^∞ design methodology is used to calculate a controller that performs well according to the criteria that have been established. Figure 10 illustrates how the controller design problem is reformulated as the standard four block H^∞ problem described in [3] — notice that the input signal x_{cont} is disregarded in the controller design which is directed towards satisfying the disturbance rejection requirement. The resulting H^∞ problem is solved using the Robust Control Toolbox[6]. Details on the use of the Robust Control Toolbox, and the algorithms it uses may be found in the User's Guide [1]. The paper of Doyle *et al.* [2] describes the key algorithm used to compute the H^∞ controller. This algorithm computes a controller C that ensures that the closed loop transfer function matrix $T_{\text{cl}}(s)$ that relates the vector of input signals $(w_1, w_2)^\top$ to the vector of output signals $(z_1, z_2)^\top$ has largest singular value $\bar{\sigma}(T_{\text{cl}})$, a function of s, bounded above by $\bar{\sigma}(T_{\text{cl}}) < 1$ uniformly on the vertical axis of the complex plane, $s = j\omega$. In order that this algorithm can be successfully applied two technical requirements need to be satisfied: the first is that the open loop transfer function matrices that relate the actuator signal V to the measured output $(z_1, z_2)^\top$, and that relate the exogenous inputs $(w_1, w_2)^\top$ to the control sensor signal I should retain full rank in the asymptotic limit as $s \to j\infty$, the second is that the open loop transfer function matrix should have neither poles nor zeros on the $j\omega$ axis. The first requirement is satisfied with the introduction of the extra input

[6]The Robust Control Toolbox is a product of The MathWorks Inc. that provides additional functionality to their software product MATLAB.

w_2 and the extra output z_2. In addition to ensuring that the rank condition is satisfied, this input-output pair introduce an extra row and column to the closed loop transfer function matrix and adds a measure of robustness to the performance measure that is already being optimized. Francis [3] shows with an application of the small gain theorem that minimizing the L^∞ norm of the closed loop transfer function relating w_3 to z_2 maximizes the size (in L^∞) of the smallest perturbation of the transfer function P_{23} that would destabilize the closed loop system. The second requirement, a restriction on the position of the open loop poles and zeros, is satisfied by using a bilinear transform of the complex plane to move the zeros of the open loop transfer function that appear at the origin to positions in the right half plane. This technique is explained in the Robust Control Toolbox guide [1].

The key to successfully using the H^∞ design method for the design of a controller that yields good closed loop performance lies in the selection of the weighting functions W^1_{in}, W^2_{in}, W^1_{out} and W^2_{out}. In the application presented in this report, the closed loop transfer function matrix that relates the inputs $(w_1, w_2)^\top$ to the outputs $(z_1, z_2)^\top$ is

$$T_{\text{cl}} = \begin{bmatrix} T_{\text{cl}\,11} & T_{\text{cl}\,12} \\ T_{\text{cl}\,11} & T_{\text{cl}\,12} \end{bmatrix}$$

with

$$\begin{aligned}
T_{\text{cl}\,11} &= W^1_{\text{out}} \left(P_{11} + \frac{P_{13} C P_{12}}{1 - C P_{23}} \right) W^1_{\text{in}} \\
T_{\text{cl}\,12} &= W^1_{\text{out}} \frac{P_{13} C}{1 - C P_{23}} W^2_{\text{in}} \\
T_{\text{cl}\,21} &= W^2_{\text{out}} \frac{P_{21}}{1 - C P_{23}} W^1_{\text{in}} \\
T_{\text{cl}\,22} &= W^2_{\text{out}} \frac{P_{23} C}{1 - C P_{23}} W^2_{\text{in}}.
\end{aligned}$$

The closed loop transfer function norms that are important for the evaluation of the design are $\|P_{11} + P_{13} C P_{12}/(1 - C P_{23})\|_\infty$, which is a measure of disturbance rejection, and $\|P_{23} C/(1 - C P_{23})\|_\infty$ which is a measure of robustness. The ideal design algorithm would produce a controller transfer function C that maintains stability in the closed loop system while minimizing a combination of the two norms, the combination being chosen to reflect the relative importance of the two criteria, disturbance rejection and robustness, at different frequencies. What the H^∞ design algorithm actually gives is a controller that minimizes the norm $\|\bar{\sigma}(T_{\text{cl}})\|_\infty$, and it is the choice of weights, W^1_{in}, W^1_{out}, W^2_{in} and W^2_{out}, that controls the relationship between the size of $\|\sigma(T_{\text{cl}})\|_\infty$ and the magnitude of the transfer functions norms that are used to evaluate system performance. In applications, the problem of choosing appropriate weights is the central problem in controller synthesis by H^∞ methods. The particular approach to design that is considered in this report

falls under the general procedure called μ-synthesis for systems with structured uncertainty which is discussed by Chiang and Safonov in [1]. Generally the problem of choosing appropriate weights is a difficult optimization problem. The usual approach to its solution is an iterative process of synthesis and either simulation or evaluation of performance measures. The designer attempts to resolve conflicting design objectives at each iteration by altering the weights. Current research in the area of μ-synthesis aims to provide tools that will help the designer in this task.

The approach taken here to the problem of choosing weights is straight-forward. The weights W^1_{in} and W^1_{out} are initially identical stable first order low-pass filters, the weights W^2_{in} and $W^2{}_{\text{out}}$ are initially identical stable first order high pass filters, and the initial choice of the filter gains ensures the existence of a solution to the initial H^∞ design problem. The H^∞ design algorithm then iteratively solves the H^∞ design problem while increasing the gain of weight W^1_{out} until a solution no longer exists. At this point the resulting design is evaluated and the closed loop transfer functions $T_{\text{cl}\,11}$, $T_{\text{cl}\,12}$, $T_{\text{cl}\,21}$, and $T_{\text{cl}\,22}$ are inspected. An adjustment of the weights, and another iteration of the procedure can improve the system performance by promoting diagonal dominance, or adjusting the relative magnitudes of the diagonal elements in the closed loop transfer function matrix.

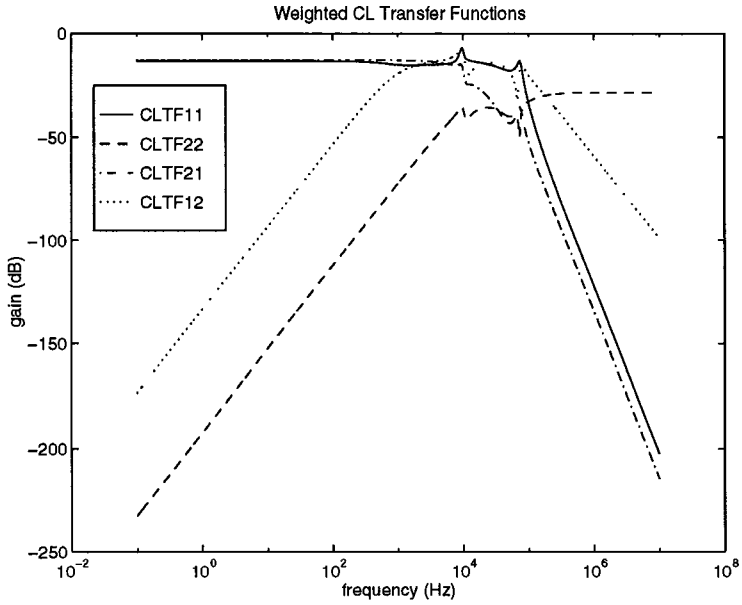

Figure 11. Closed Loop Transfer functions $T_{\text{cl}\,ij}$

The Matlab M-file that is used for the computation of the controller is given in Appendix C. The M-file calls two other files, `Toolpost.m` and `Lathe.m` to calculate the models for the toolpost and the lathe. `Toolpost.m` is listed in Appendix A, and

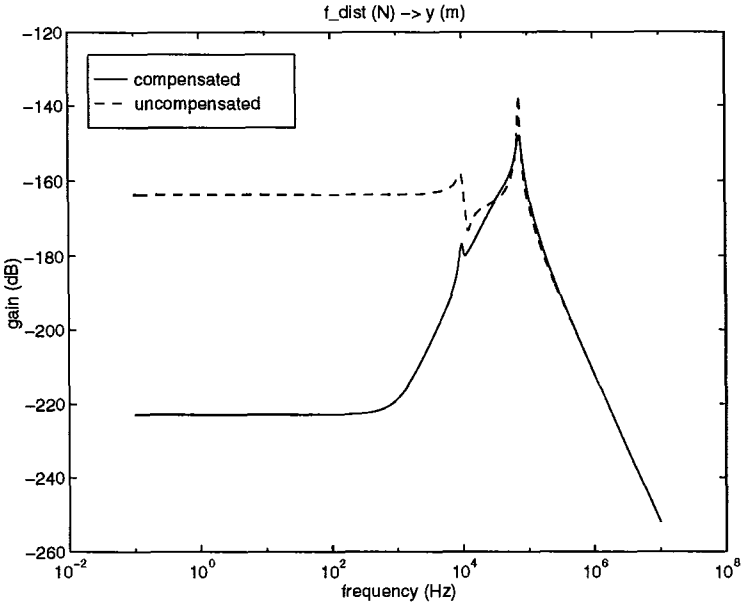

Figure 12. Closed loop transfer function $f_{\text{dist}} \rightarrow y$

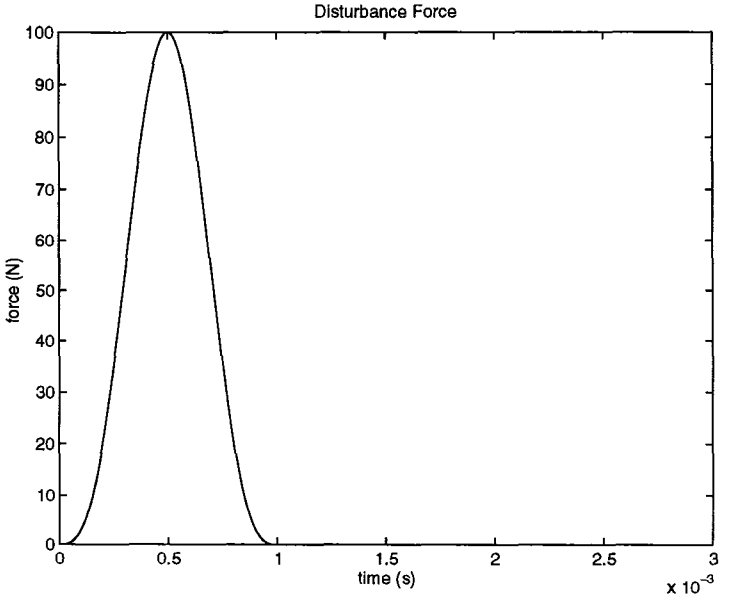

Figure 13. Disturbance signal $f_{\text{dist}}(t)$

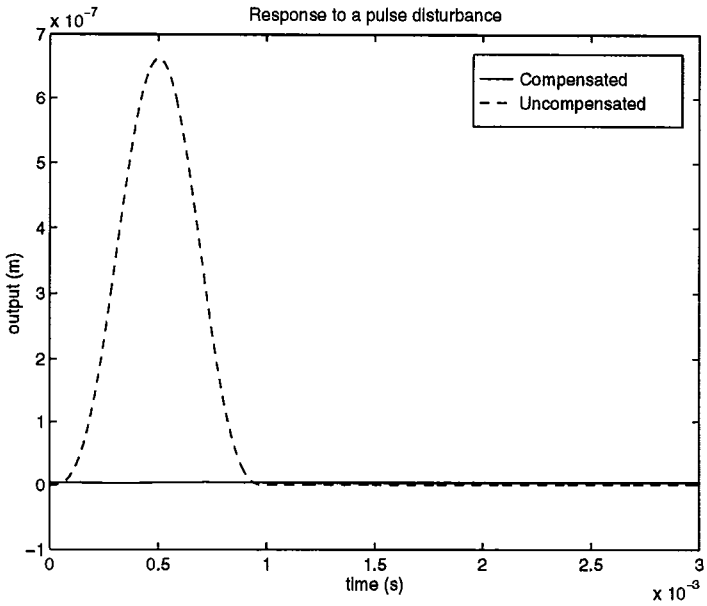

Figure 14. Closed loop response to disturbance $y(t)$

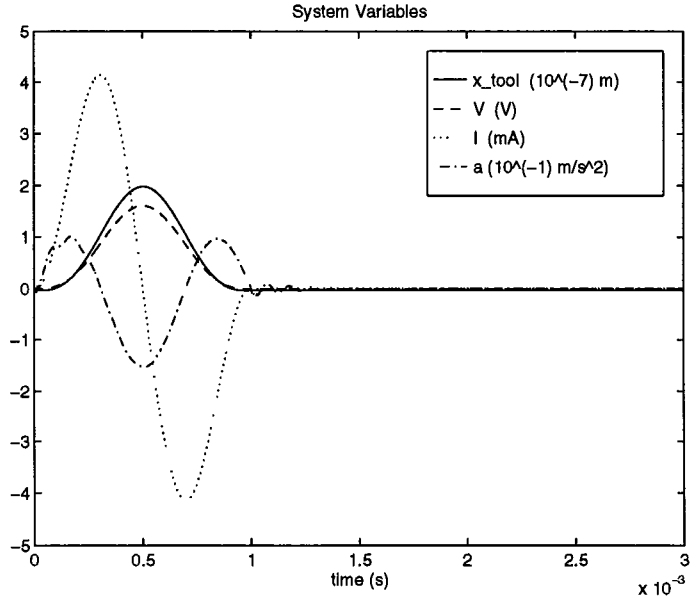

Figure 15. Signal magnitudes in response to disturbance

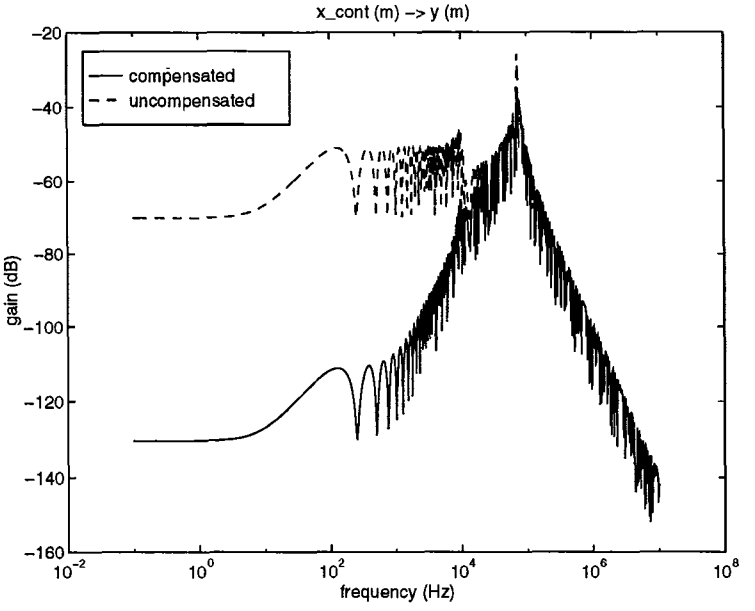

Figure 16. Closed loop transfer function $x_{\text{cont}} \rightarrow y - x_{\text{cont}}$

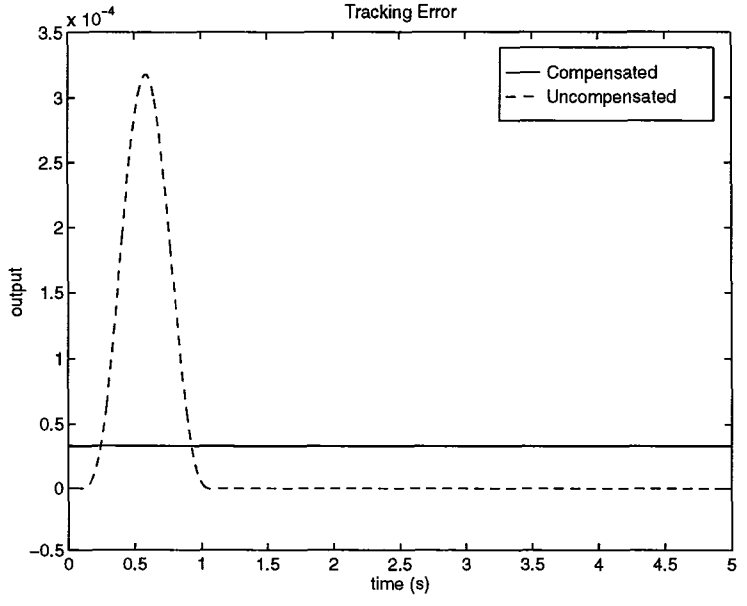

Figure 17. Tracking error with respect to a control signal x_{cont} of unit amplitude

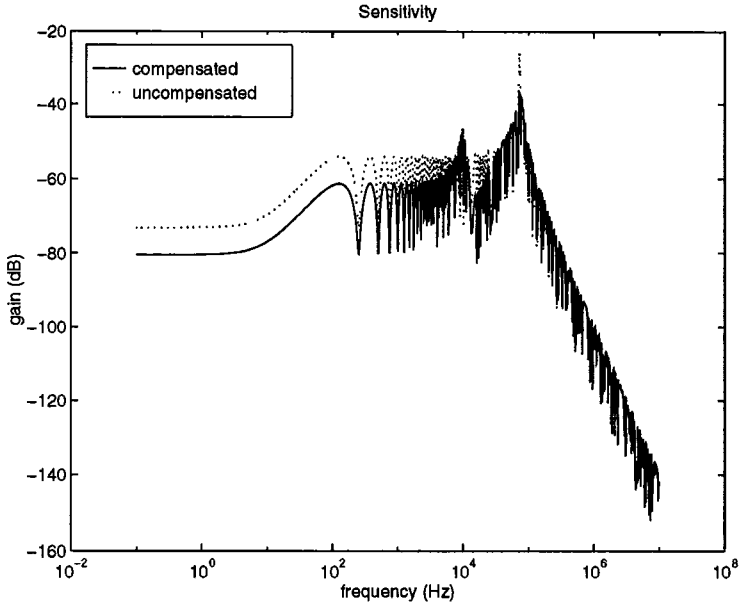

Figure 18. Closed loop sensitivity for the lathe-toolpost loop

`Lathe.m` produces a low dimensional state-space approximation to the transcendental Lathe transfer functions of the Lathe model in Appendix B. The closed loop transfer functions and system responses illustrated in Figures 12 to 18 are calculated in the frequency domain with a system model that is composed of the lathe model of Appendix B, the toolpost model of Appendix A, and the Controller that is calculated in C. An important practical consideration that arises when performing computations is that of numerical conditioning. The M-file that calculates the controller includes model reduction of both the open loop plant model and the final computed controller to improve conditioning in both the controller design algorithm and the subsequent system performance calculations.

The results of the design are presented in figures 11 to 18. The first figure gives an indication of which elements in closed loop transfer function matrix are contributing to the singular value $\bar{\sigma}(T_{cl})$. The first column of the matrix dominates at low frequencies, and the entry $T_{cl\,22}$ dominates at high frequencies. Figures 12 to 15 illustrate the System performance with respect to disturbance rejection. The transfer function plot in Figure 12 shows 40 dB improvement in disturbance rejection for frequencies up to 1 kHz for the actively compensated toolpost when compared to the performance of the toolpost with open circuited actuator. At 5 kHz, the actively controlled system still shows about 30 dB of improvement. This improvement is again illustrated in Figure 14 which compares the response of the compensated system to a pulse shaped disturbance force with the response of the uncompensated system to the same disturbance. Figure 15 plots the important signals associated with the closed loop system as it experiences the disturbance force plotted in Figure 13. These signals scale linearly with the magnitude of the disturbance pulse (since the model is linear) and provide a useful estimate of dynamic range required in the various system components. The tracking performance of the system is illustrated in Figures 16 and 17. Figure 16 shows that the compensated system displays a 60 dB improvement in tracking between 10^{-1} Hz and 10 Hz, and Figure 17 shows the response of the tracking error signal to a low-bandwidth unit pulse signal on the position control input x_{cont}. The anomalous D.C. offset that appears in the compensated response is an artifact of the computation, there is a loss of accuracy in the transfer function computations for frequencies close to zero. Finally, Figure 18 compares the sensitivity functions associated with the lathe-toolpost loop for the compensated and uncompensated toolposts. The magnitude of this transfer function is inversely related to a lower bound on the size of perturbation that would be needed in the open loop transfer function to destabilize the closed loop system. It can be seen from the graph that the compensator sightly improves this measure of robustness.

6 CONCLUSIONS AND RECOMMENDATIONS FOR FUTURE WORK

In this report a simple, linear, system model has been developed for the design of an active toolpost, and the model has been used as a basis for a controller design for that toolpost. The principal conclusions that come out of this work are, that active control of toolpost vibration is a feasible way to improve the quality of the surface finish in turning operations, and that the toolpost design considered in this report is a good candidate for active vibration suppression. The results presented show that under the assumptions made, a compensated toolpost is able to provide a high degree of disturbance rejection in the cutting process without sacrificing robust stability or accuracy. Furthermore, an analysis of the signal amplitudes associated with the toolpost model indicate that during normal operation the tool-post components are operating well within their designed ranges. It is worth stressing that the promising nature of the results presented here should not be regarded as the proof of a successful design, but rather as strong justification for continued refinement and evaluation of the current design. In particular, there are several areas where the rather severe assumptions made in this report need to be more closely examined.

The first of these are the assumptions that were made in the introduction about the causes of vibration in the cutting process. Two types of vibration were mentioned there, one the result of instabilities combining with non-linear dynamics to produce limit cycle trajectories, and the other the result of amplification of exogenous disturbances in the cutting force. Because the models developed in this paper are all linear, the first type of vibration is only considered tangentially by placing requirements on robust stability of the linear model — a more thorough consideration would require an investigation of the nonlinear dynamics associated with the cutting process. The second type of vibration is dealt with directly by incorporating exogenous disturbances to the cutting force in the lathe model of Section 4. Suppression of this source of vibration is a problem in disturbance rejection, and in order to gauge the effectiveness of a design with respect to this criterion it is necessary to have an accurate model of the expected disturbance signals. Such a model should be built on experimental data from cutting tests.

A second group of assumptions that need careful evaluation are the assumptions that were made about system components in order to produce a linear model. The three places where these assumptions are likely to have the greatest impact on system behavior are in the actuator model, the model of the lathe dynamics, and the model of the cutting process. The model of the actuator presented in Section 2 is calculated from typical linear constitutive parameters for PZT material a more accurate model should be obtained from an experimental study of the actual actuators that are to be used. In particular, attention should be paid to the operating range over which a linear model is valid, and to the effect on the device of power dissipation and the heating associated with it. The lathe dynamics affect the system by restricting the bandwidth over which control is achievable. In Section 4 the

complicated dynamics associated with the dynamics of the workpiece and the lathe machinery is modeled by a simple one degree of freedom system. Accurate model of the lathe dynamics, and the dynamics of the cutting process are, of course, an unrealistic expectation, and not really needed, what is needed though is an accurate estimate of the bandwidth over which the simple second order model is accurate, and an estimate of the sensitivity of the system model to the incremental stiffness k_c that relates cutting force to chip-load. Both the lathe model and the model of the cutting process are highly dependent on the details of a specific cutting operation, and a desirable feature of an improved controller would be an ability to estimate these models and adaptively alter the control law.

Another area for future work is the design of the physical implementation of the controller. The intention has been to implement the controller in a digital signal processing chip with an effective bandwidth in the high audio range. This choice permits the use of commercial signal processing boards that interface with personal computers. The highest frequency poles in the controller that was described in Section 5 have frequencies near 4×10^4 kHz, which is at the high end of this range, and it may be that some performance has to be sacrificed if the controller bandwidth needs to be reduced.

Finally, although the work described in this report is my own, it was undertaken as part of a larger project, the ARPA SMS project. I would like to acknowledge the useful interaction that I have had over the past year with the other members of the project team. In particular I would like to thank Professor Guangming Zhang, his team of graduate students, undergraduate students and post-docs, and Mark Regelbrugge of Lockheed, who have listened to, read, and discussed many presentations of parts of this work over the past year, and my advisor Professor John Baras who has supported me during this project.

A M-FILE FOR TOOLPOST MODEL

```
% This file contains linear models for the toolpost and the actuator.
%
% The system schematic for the Toolpost with actuator is given by
%     the diagram
%
%             ------------------------------------------------
%             |                                  ------------     |
%            1|                               1|            |2   |2
%    f_cut ---|--------------------------------|            |----|-- a_tool
%             |      ------------              |            |    |
%            2|    2|            |1          2| Toolpost   |    |
%    V_in  ---|-----|            |------------|            |1   |1
%             |     | Actuator   |            |            |----|-- x_tool
%             |     | and Drive  |            |------------| |  |
%             |    1|            |2                        |  |3
%             |  ---|            |-------------------------|-- I_act
%             |  |  |------------|                         |  |
%             |  |_____________________________________________|  |
%             |                                                   |
%             |___________________________________________________|
%
%       The numbers on the signal lines give the index of the
%       signal in the correponding input and output signal vectors
%

% Actuator Parameters and constants

epsilon_0 = 8.85 * 10^(-12);

L = 1.8 * 10^(-2);
R = 3.5 * 10^(-3);
N = 150;

K = 1300;
d = 350 * 10^(-12);
Y = 9.9 * 10^(10);

Area = pi*R^2;

% Drive circuit parameters
A_ol = 10^5;
R_1 = 2 * 10^3;
R_2 = 28 * 10^3;
R_s = 10;
```

```
% Toolpost mechanical structural parameters

K_act = Area * K*epsilon_0 * Y/(L*(K*epsilon_0 + d^2*Y));

%M_1 = 0.2;
M_1 = 0.04;  % Value calculated from measured resonance and measured
             %   stiffness  --- see Nov Report.
M_2 = 0.01;
%K_1 = K_act/10;
K_1 = 5 * 10^6;  % Value measured from toolpost -- see Nov Report
K_2 = K_act/100;
xi_1 = .1;
xi_2 = .1;

% Toolpost computed coefficients

C_1 = sqrt(4 * K_1 * M_1 * xi_1^2/(1 - xi_1^2));
C_2 = sqrt(4 * K_2 * M_2 * xi_2^2/(1 - xi_2^2));

omega_1 = sqrt(C_1^2 - 4 * K_1 * M_1)/(2*M_1);
omega_2 = sqrt(C_2^2 - 4 * K_2 * M_2)/(2*M_2);

% Actuator computed coefficients

P_11 = -L/(Area*Y);
P_12 = d*L/(N*Area*K*epsilon_0);
P_21 = P_12;
P_22 = L/(N^2*Area*K*epsilon_0);


A_11 = - L/(R_s*N^2*Area*K^2*epsilon_0^2)*...
          (K*epsilon_0 + d^2*Y) * (1 + A_ol*R_1/(R_1 + R_2));
B_11 = d*Y/(R_s*N*K*epsilon_0)*(1 + A_ol*R_1/(R_1 + R_2));
B_12 = A_ol*R_2/(R_s*(R_1 + R_2));


% Actuator Model

Aact = [A_11];
Bact = [B_11, B_12];
Cact = [d*Y/(N*K*epsilon_0), A_11]';
Dact = [-Area*Y/L, 0; B_11, B_12];
```

```
% Toolpost computed coefficients;

Alpha = 1 + A_ol*R_1/(R_1 + R_2);
Beta = P_21*P_12/P_11;
Gamma = A_ol*R_2/(R_1 + R_2);
Delta = P_22 - P_12*P_21/P_11;

K_tool = K_2/(K_2^2 - K_2*(K_1+K_2));


% Toolpost Model

Amech = [ -C_1/M_1        ,     -K_1/M_1
             1            ,        0      ];

Bmech = [ -1/M_1, 1/M_1
            0   ,  0    ];

Cmech = [       0        ,          1
           -C_1/M_1,           -K_1/M_1  ];

Dmech = [0, 0
         -1/M_1, 1/M_1];

Ain = [];
Bin = [];
Cin = [];
Din = [1,0;0,0;0,0;0,1];

Aout = [];
Bout = [];
Cout = [];
Dout = [1,0,0,0
        0,1,0,0
        0,0,0,1];

%
%  Construct Toolpost with controller
%  final model has 2 inputs and 3 outputs
%       inputs :  f_cut     outputs: x_act
%                 V_in               a_tool
%                                    I_act
%

[Atool,Btool,Ctool,Dtool] = ...
        append(Amech,Bmech,Cmech,Dmech,Aact,Bact,Cact,Dact);

[Atool,Btool,Ctool,Dtool] = cloop(Atool,Btool,Ctool,Dtool,[1,3],[3,2]);

[Atool,Btool,Ctool,Dtool] = ...
        series(Ain,Bin,Cin,Din,Atool,Btool,Ctool,Dtool);

[Atool,Btool,Ctool,Dtool] = ...
        series(Atool,Btool,Ctool,Dtool,Aout,Bout,Cout,Dout);
```

```
K_11 = - P_11*Delta/(Delta*(K_1*P_11 - 1) - Beta);
K_12 =  - P_12*Gamma/(Alpha*(K_1*P_11*Delta  - (Delta + Beta)));
K_31 = P_21/(K_1*P_11*Delta - (Delta + Beta));
K_32 = Gamma*(K_1*P_11 - 1)/(Alpha*(K_1*P_11*Delta - (Delta + Beta)));


% Toolpost model for open circuit condition on Actuator
% inputs to actuator are (x,I) and outputs are (f,V)

A_open = [1e-15];

B_open = [0,1];

C_open = [Y*d/(N^2*K*epsilon_0); L*(d^2*Y + N*K)/(N^3*K^2*Area*epsilon_0)];

D_open = [-Area*Y/L, 0; -d*Y/(N*K*epsilon_0), 0];

% Combine with mechanical model

[Atool_op,Btool_op,Ctool_op,Dtool_op] = ...
        append(Amech,Bmech,Cmech,Dmech,A_open,B_open,C_open,D_open);

[Atool_op,Btool_op,Ctool_op,Dtool_op] = ...
        cloop(Atool_op,Btool_op,Ctool_op,Dtool_op,[1,3],[3,2]);

[Atool_op,Btool_op,Ctool_op,Dtool_op] = ...
        series(Ain,Bin,Cin,Din,Atool_op,Btool_op,Ctool_op,Dtool_op);

[Atool_op,Btool_op,Ctool_op,Dtool_op] = ...
        series(Atool_op,Btool_op,Ctool_op,Dtool_op,Aout,Bout,Cout,Dout);
```

B M-FILE FOR LATHE MODEL

```
function answer = Tlathe(s)

% Returns a matrix with columns [T_11, T_12, T_21, T_22] where each
% column is a transfer function evaluated at the frequencies in the
% input vector s

sz = size(s); if sz(2)>sz(1) size = size'; end;
%
%       Cutting Process
%
% The model used for the cutting process is a simple model that treats
% the variation in cutting force as a linear function of the variation
% in depth of cut. The proportionality constant K_c is taken from
% Guangming Zhang's PhD dissertation and applies to machining of
% aluminium pieces of fixed diameter. The cutting parameters are

N = 2400;  % Cutting speed (rpm)
f = 1.5;  % feed rate (mm/rev)
d = 0.05;  % depth of cut (mm)

% and the empirical formula for the cutting stiffness in N/m is

k_c = 1000 * 7500/(f^(0.15)*N^(0.05))* d;

% Note, Guangming Zhang states that the units in the paper are N/mm,
%       hence the extra factor of 1000 in the above formula.

%Lathe Parameters

mu = 0.8;  % Overlap factor
tau = 60/N; % Transport delay associated with one revolution of the workpiece

K = 5.0 *10^8;          % Stiffness of Lathe structural mode
omega = 10000;          % Natural frequency of structural resonance
M = (k_c + K)/(omega^2);        % Equivalent mass of Lathe structural mode
xi = 0.1;               % Percent damping of Lathe structural mode
C = 2*xi*sqrt(K*M);     % viscous parameter for Lathe structural mode

term1 =  k_c*(1 - mu*exp(-s*tau));
term2 = M*s.^2 + C*s + K;
denom = term1 + term2;

% answer = [T_11, T_12, T_21, T_22]
answer = [1./denom, -term2./denom, term2./denom, term1.*term2./denom];

return
```

C M-FILE FOR CONTROLLER DESIGN

```
% This file produces an Hinfty controller for the Toolpost
% problem. The block diagram for the augmented plant is as follows
%
```

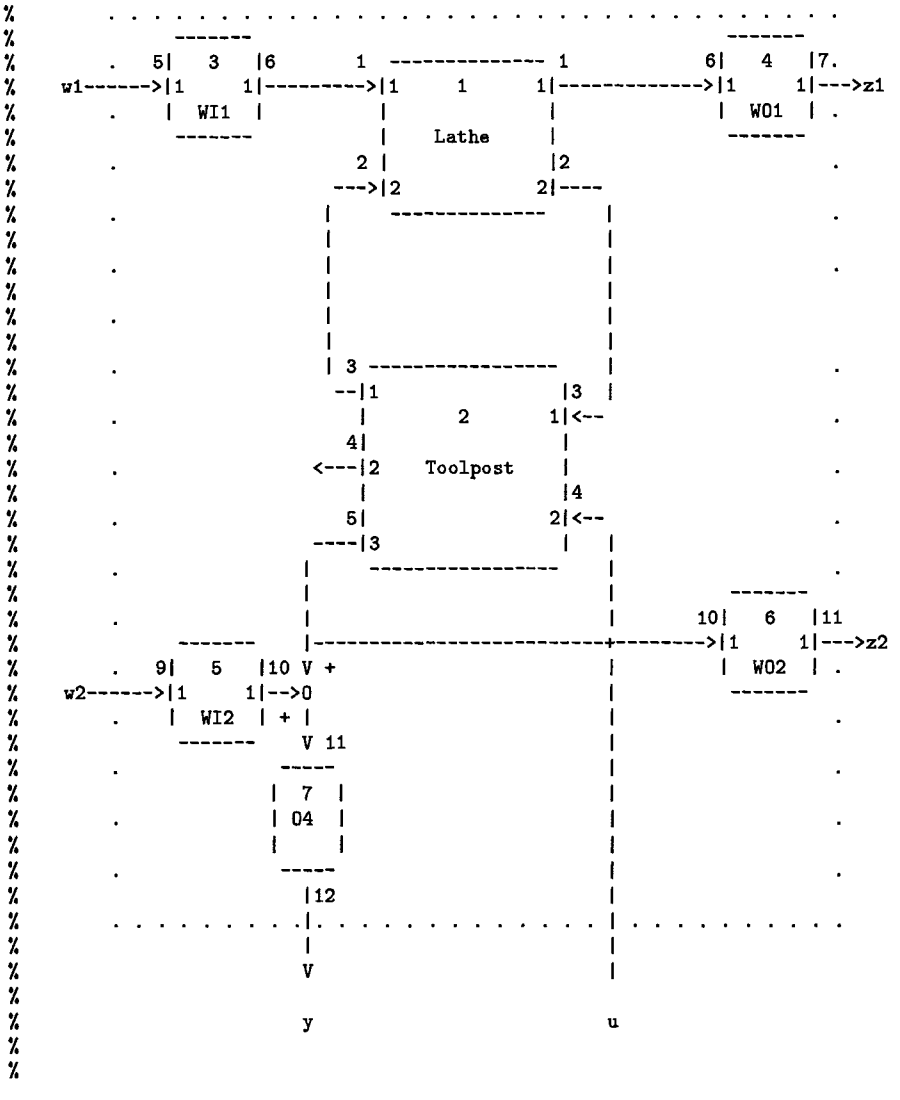


```
Toolpost;
Lathe;
```

```
% Make the weights and ancillary blocks

AI4 = [];
BI4 = [];
CI4 = [];
DI4 = [1];

nu1 = 10^3;
nu2 = 10^4;
nu3 = 10^3;
nu4 = 10^4;

rho_1 = 1 * 10^(5);
rho_2 = 0.1;

nWI1 = rho_1*[0 , 1];
dWI1 = [1/nu1, 1];
[AWI1, BWI1, CWI1, DWI1] = tf2ss(nWI1,dWI1);

nWO1 = rho_1*[0 , 1];
dWO1 = [1/nu1, 1];
[AWO1, BWO1, CWO1, DWO1] = tf2ss(nWO1,dWO1);


nWI2 = 1/3*rho_2*[1/nu3, 1, 0];
dWI2 = [1/nu4, 1+nu2/nu4, nu2];
 [AWI2, BWI2, CWI2, DWI2] = tf2ss(nWI2,dWI2);

%nWO2 = 3*rho_2*[1/nu4, 1, 0];
%dWO2 = [1/nu3, 1+nu2/nu3, nu2];
% [AWO2, BWO2, CWO2, DWO2] = tf2ss(nWO2,dWO2);

nWO2 = 3*rho_2*[1/nu4, 0];
dWO2 = [1/nu3, 1];
 [AWO2, BWO2, CWO2, DWO2] = tf2ss(nWO2,dWO2);


% Connect the toolpost and lathe together and perform model reduction

[Ap, Bp, Cp, Dp] = append(...
        A_lathe, B_lathe, C_lathe, D_lathe,...
        Atool, Btool, Ctool, Dtool);

Q = [2,3;3,2];
Inputs = [1, 4];
Outputs = [1, 5];

[Ap, Bp, Cp, Dp] = connect(Ap, Bp, Cp, Dp, Q, Inputs, Outputs);
[ab,bb,cb,db,totbnd,hsv] = schmr(Ap,Bp,Cp,Dp,3);
```

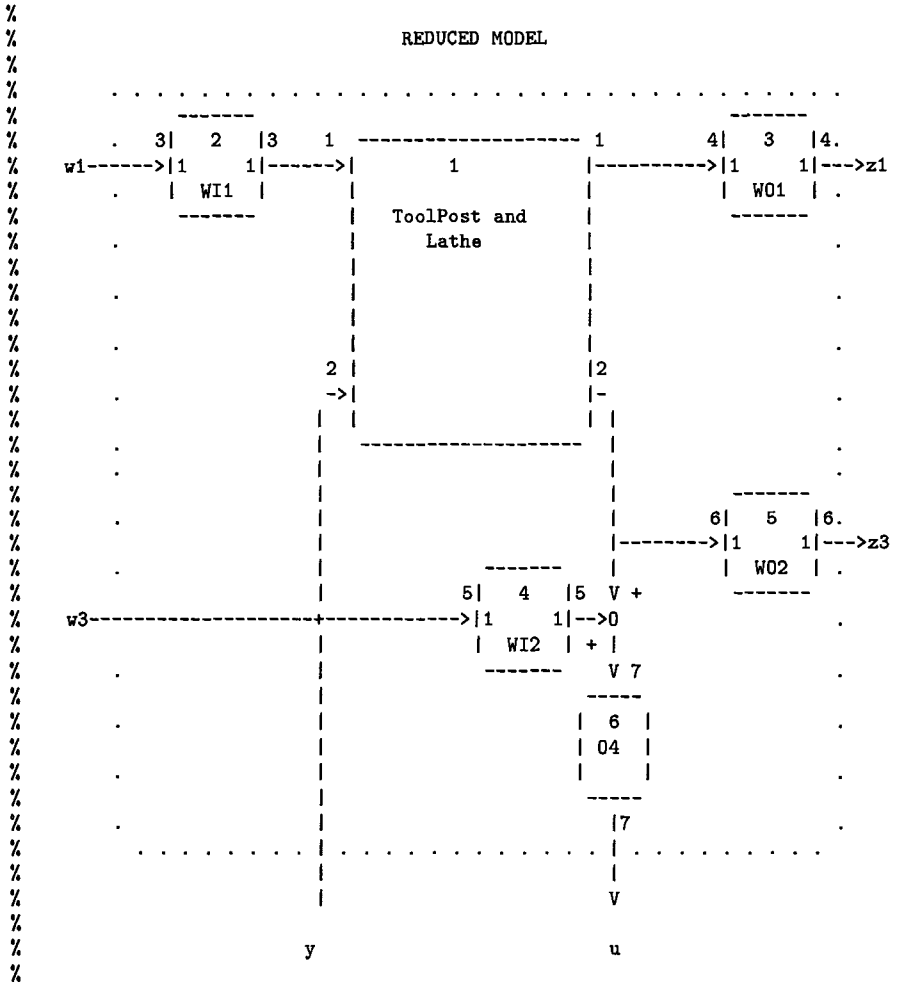


```
% Add input and output weights

[Ap, Bp, Cp, Dp] = append(Ap, Bp, Cp, Dp, AWI1, BWI1, CWI1, DWI1);
[Ap, Bp, Cp, Dp] = append(Ap, Bp, Cp, Dp, AWO1, BWO1, CWO1, DWO1);
[Ap, Bp, Cp, Dp] = append(Ap, Bp, Cp, Dp, AWI2, BWI2, CWI2, DWI2);
[Ap, Bp, Cp, Dp] = append(Ap, Bp, Cp, Dp, AWO2, BWO2, CWO2, DWO2);
[Ap, Bp, Cp, Dp] = append(Ap, Bp, Cp, Dp, AI4, BI4, CI4, DI4);
```

```
Q = [1, 3, 0; 4, 1, 0; 6, 2, 0; 7, 2, 5];
Inputs = [3, 5, 2];
Outputs = [4, 6, 7];


[Ap, Bp, Cp, Dp] = connect(Ap, Bp, Cp, Dp, Q, Inputs, Outputs);


% The Augmented system has a zero at the origin which causes problems
%   when calculating Hinfty controllers so we introduce a Bilinear
%   transform of the Augmented plant to better condition the problem
%

%Parameters for Bilinear Transform

p_1 = 10;
p_2 = 10^10;

[Ap,Bp,Cp,Dp] = bilin(Ap,Bp,Cp,Dp,1,'Sft_jw',[p_2,p_1]);


%Partition system for hinfty function

A = Ap;
B1 = Bp(:,[1, 2]);
B2 = Bp(:,3);
C1 = Cp([1, 2],:);
C2 = Cp(3,:);
D11 = Dp([1,2],[1,2]);
D12 = Dp([1,2],3);
D21 = Dp(3,[1,2]);
D22 = Dp(3,3);



TSS_P = mksys(A, B1, B2, C1, C2, D11, D12, D21, D22, 'tss');

[rho_opt, ss_f, ss_cl] = hinfopt(TSS_P,1);

[Af,Bf,Cf,Df] = branch(ss_f);
[Acl,Bcl,Ccl,Dcl] = branch(ss_cl);

%Transform Controller Back
[Af,Bf,Cf,Df] = bilin(Af,Bf,Cf,Df,-1,'Sft_jw',[p_2,p_1]);
[Acl,Bcl,Ccl,Dcl] = bilin(Acl,Bcl,Ccl,Dcl,-1,'Sft_jw',[p_2,p_1]);
```

```
% Reduce Controller Order

[Af,Bf,Cf,Df,totbnd,hsv] = schmr(Af,Bf,Cf,Df,3);


[Atool2,Btool2,Ctool2,Dtool2] = ...
        append(Atool,Btool,Ctool,Dtool,Af,Bf,Cf,Df);
[Atool2,Btool2,Ctool2,Dtool2] = ...
        cloop(Atool2,Btool2,Ctool2,Dtool2,[3,4],[3,2]);

Compensator = mksys(Af, Bf, Cf, Df, 'ss');

save Compensator Compensator;
```

References

[1] Richard Y. Chiang and Michael G. Safonov. *Robust Control TOOLBOX For Use with MATLAB User's Guide.* The MathWorks, 1992.

[2] John C. Doyle, Keith Glover, Pramod P. Khargonekar, and Francis Bruce A. State-space solutions to standard H_2 and H_∞ control problems. *IEEE Transactions on Automatic Control*, 34:831 – 846, 1989.

[3] Bruce A. Francis. *A course in H^∞ control theory.* Springer Verlag, first edition, 1987.

[4] H. E. Merritt. Theory of self-excited machine-tool chatter. *Journal of Engineering for Industry*, pages 447–454, November 1965. ASME Paper No. 64-WA/Prod-13.

[5] Guangming Zhang. *Dynamic modelling and dynamic analysis of the boring machine system.* PhD thesis, University of Illinois, 1986.